Available online at www.sciencedirect.com
ScienceDirect
Journal of the European Ceramic Society 28 (2008) 3141–3148
www.elsevier.com/locate/jeurceramsoc

# The influence of tetrahedral ordering on the microwave dielectric properties of $Sr_{0.05}Ba_{0.95}Al_2Si_2O_8$ and $BaM_2M'_2O_8$ (M = Al, Ga, M′ = Si, Ge) ceramics

Marjeta Macek Krzmanc *, Boštjan Jančar, Danilo Suvorov

*Advanced Materials Department, "Jožef Stefan" Institute, Jamova 39, 1000 Ljubljana, Slovenia*

Received 31 March 2008; received in revised form 19 May 2008; accepted 27 May 2008
Available online 3 July 2008

**Abstract**

The feldspars $Sr_{0.05}Ba_{0.95}Al_2Si_2O_8$, $BaAl_2Ge_2O_8$ and $BaGa_2Si_2O_8$ with S.G. I2/c, and $BaGa_2Ge_2O_8$ with S.G. $P2_1/a$, were studied by means of crystal structural and microstructural analyses and dielectric measurements. All the investigated densely sintered single-phase feldspars exhibited a permittivity ($\varepsilon$) of 7–8 and a temperature coefficient of resonant frequency ($\tau_f$) from −20 to −30 ppm/°C. In contrast to the $\varepsilon$ and $\tau_f$ the dielectric losses were found to be dependent on the annealing conditions. In $Sr_{0.05}Ba_{0.95}Al_2Si_2O_8$ the Qxf values increased from 42,500 to 92,600 GHz when the annealing time at 1400 °C was increased from 1 to 162 h. Such a difference in the Qxf values as a result of various annealing conditions was attributed to different degrees of tetrahedral ordering. In contrast to aluminosilicate feldspars, Ge-containing feldspars can be sintered and ordered at low temperature. In $BaAl_2Ge_2O_8$ the Qxf values decreased when the sintering temperature exceeded the order-disorder I2/c ↔ C2/m phase-transition temperature. The $BaGa_2Si_2O_8$ and $BaGa_2Ge_2O_8$ feldspars exhibited a rapid decrease of Qxf values when the annealing temperature approached the melting point. However, the $BaAl_2Ge_2O_8$ and $BaGa_2Ge_2O_8$ can regain their high Qxf values by annealing at 1000 °C. The $BaGa_2Ge_2O_8$ stood out from the other investigated feldspars, with a sintering temperature of 1100 °C, Qxf values of 100,000–150,000 GHz and a $\tau_f$ of −26 ppm/°C.


*Keywords:* A. Powder solid-state reactions; B. X-ray methods; C. Dielectric properties; D. Silicate; E. Substrates

## 1. Introduction

Thanks to the development of new materials and new electronic components mobile telecommunication technologies, such as mobile phones and wireless LANs, have made great progress over the past 20 years. The current trend in mobile telecommunications is to broaden the utilized frequency range to include higher frequencies (>10 GHz).[1,2] For applications at frequencies >10 GHz low-permittivity materials are more appropriate than high-permittivity materials. The reason is the small size of high-permittivity materials at high frequencies, which requires very accurate processing.[1] Low-permittivity materials are currently used as substrate materials in the low-temperature co-fired ceramic (LTCC) technology.[1,3,4] There are several types of LTCC substrate materials, which are described in detail in reference.[4] One of them is the Motorola advanced dielectric, prepared from lead-free glass ($B_2O_3$, $K_2O$, $SiO_2$, CaO, SrO, BaO), $Al_2O_3$ as a ceramic filler and $TiO_2$ for the adjustment of the temperature coefficient of the resonant frequency. In the first step the role of the glass is to increase the densification. In the second step the glass reacts with $Al_2O_3$ and forms feldspar-type crystalline phases $MeAl_2Si_2O_8$ (Me = Ca, Sr or Ba).[4] In the course of this reaction the amount of glass is greatly reduced, but not completely eliminated. Due to the presence of a glassy phase such substrates exhibit much higher dielectric losses compared to fully crystalline $MeAl_2Si_2O_8$ (Me = Ca, Sr, Ba) feldspars. Despite the use of these feldspars as ingredients of LTCC dielectric substrates, the dielectric properties of these materials have never been studied in such detail as those of the perovskites. Several studies dealing with the microwave dielectric properties of perovskites revealed the important influence of structural order on the dielectric losses.[5–7] Like with perovskites an increase in the structural order is expected to result in a Q-factor improvement in these materials with their different crystal structures.

The aluminosilicate feldspars are the most abundant minerals in the earth's crust, and because of that they have been thoroughly

* Corresponding author. Tel.: +386 1 477 3481; fax: +386 1 477 3875.
*E-mail address:* marjeta.macek@ijs.si (M.M. Krzmanc).

0955-2219/$ – see front matter © 2008 Elsevier Ltd. All rights reserved.
doi:10.1016/j.jeurceramsoc.2008.05.024

investigated by mineralogists. The feldspar crystal structure is composed of a 3D framework of corner-shared tetrahedra that are centered by $Si^{4+}$ ($Ge^{4+}$) and $Al^{3+}$ ($Ga^{3+}$). Large alkali ($Na^+$, $K^+$) or alkaline-earth ions ($Ca^{2+}$, $Sr^{2+}$, $Ba^{2+}$) in the interstices balance the charge caused by the different charges of the tetrahedral $Al^{3+}$ ($Ga^{3+}$) and $Si^{4+}$ ($Ge^{4+}$) ions. All the feldspars have low symmetry; they are either triclinic or monoclinic. The symmetry of the lattice depends on the effective size of the large cations ($Na^+$, $Ca^{2+}$, $Ba^{2+}$) and the distribution of the tetrahedral ions ($Al^{3+}$, $Si^{4+}$). The feldspars with smaller cations ($Na^+$, $Ca^{2+}$) are triclinic, whereas the larger cations ($Sr^{2+}$, $Ba^{2+}$) tend to support the monoclinic symmetry.[8]

Feldspars are known to undergo several phase transitions, which are of the order-disorder or displacive type. Among the feldspars, the plagioclase feldspars ($Na_xCa_{1-x}Al_{2-x}Si_{2+x}O_8$) and their tetrahedral Al, Si ordering have been the most intensively investigated. Through various studies of the mechanisms and kinetics of the tetrahedral ordering, mineralogists have tried to get an insight into the geological history of the earth. During their studies they had to contend with the sluggishness of the tetrahedral Al, Si ordering and the small differences in the X-ray scattering efficiencies of Al and Si. The slow tetrahedral ordering in the aluminosilicate feldspars is a consequence of the strong Si–O bond. $MeAl_2Si_2O_8$ (Me = Ca, Sr, Ba) feldspars remain essentially ordered at all temperatures below the melting point. $BaAl_2Ge_2O_8$ is the only known feldspar with a I2/c → C2/m order-disorder phase transition below the melting point. Due to the weaker Ge–O bond, compared to the Si–O bond, the tetrahedral ordering kinetics in $BaAl_2Ge_2O_8$ is enhanced compared to the ordering in $MeAl_2Si_2O_8$ (Me = Ca, Sr, Ba).[9,10] The results of our previous studies, which showed that $MeAl_2Si_2O_8$ (Me = Ca, Sr, Ba) requires long heat-treatment times to attain high Qxf values, were in accordance with the slow tetrahedral ordering.[11] We also found that the Qxf values of the $MeAl_2Si_2O_8$ (Me = Ca, Sr, Ba) materials decrease in the following order: $BaAl_2Si_2O_8 > SrAl_2Si_2O_8 > CaAl_2Si_2O_8$. Monoclinic $BaAl_2Si_2O_8$ exhibits an order-higher Qxf value (40,000–90,000 GHz) compared to the triclinic $CaAl_2Si_2O_8$ (6,000–11,000 GHz).[11,12] This and the faster ordering kinetics of Ge-substituted feldspars, got us interested in the study of other tetrahedrally substituted feldspars. The sintering temperature was also expected to be lower in the case of $BaAl_2Ge_2O_8$ and $BaGa_2Ge_2O_8$. All these facts and the promising dielectric properties of $BaAl_2Si_2O_8$ focused our work on a systematic study of the correlations between structural ordering and the microwave dielectric properties of $Sr_{0.05}Ba_{0.95}Al_2Si_2O_8$ and $BaM_2M'_2O_8$ (M = Al, Ga, M′ = Si, Ge) feldspars.

## 2. Experimental

The $Sr_{0.05}Ba_{0.95}Al_2Si_2O_8$ and $BaM_2M'_2O_8$ (M = Al, Ga, M′ = Si, Ge) ceramics were synthesized using solid-state reaction techniques. Stoichiometric mixtures of reagent-grade oxides and carbonates were homogenized and then repeatedly pre-reacted up to the single-phase formation of the desired phase. Prior to sintering the powders were milled with Y-stabilized $ZrO_2$ milling balls to a median particle size of 0.8 μm and then isostatically pressed at ∼700 MPa. The details of the firing and sintering conditions can be seen in Table 1. The cooling rate from the sintering temperature ($T_s$) was either fast or slow, with the latter being a controlled cooling rate of 0.7 °C/min. Fast cooling refers to uncontrolled cooling in the furnace as a result of natural convection, conduction and radiation from the sintering temperature to room temperature. The $BaAl_2Ge_2O_8$ resonators and capacitors were sintered while muffled with powder of the same composition. Using this technique it was possible to prevent most of the evaporation of $GeO_2$ from the surface of the pellet.

The progress of the reaction after each pre-reaction step was monitored by powder X-ray diffraction (XRD) (Bruker AXS, D4 Endeavor). The X-ray powder-diffraction data were collected from $10° < 2\theta < 60°$ with a step of 0.04°, a counting time of 4 s, and a variable V12 slit. For the determination of the unit-cell volume ($V$) the XRD data were collected from $5° < 2\theta < 90°$ with a step of 0.02°, a counting time of 10 s, and a variable V12 slit. The TOPAS R program was used for the determination of the unit-cell volumes of the synthesized feldspars with a Rietveld refinement of the X-ray powder-diffraction data. In order to determine the unit-cell volume the structures of the synthesized feldspars were fitted on the basis of known ICSD data for $BaAl_{1.9}Si_{2.06}O_8$ (ICSD 27528), $BaAl_2Ge_2O_8$ (ICSD 1282), $BaGa_2Si_2O_8$ (ICSD 163) and $BaGa_2Ge_2O_8$ (ICSD 368).[13] During the refinement all the structural parameters, except the unit-cell parameters, were kept fixed. In the case of $Sr_{0.05}Ba_{0.95}Al_2Si_2O_8$ the known structural data for $BaAl_{1.9}Si_{2.06}O_8$ (ICSD 27528) were modified to take into account the right composition. The molar volume ($V_m$) was calculated from the unit-cell volume with the equation $V_m = V/Z$, where $Z$ represents the number of formula units in a single unit cell.

In order to check the repeatability and to compare the structural and dielectric properties from different synthesis runs, the synthesis of all the feldspars in this study was performed twice.

The densities of the sintered specimens were measured using Archimedes' method with distilled water. The theoretical den-

Table 1
Thermal treatments and sintering conditions of studied feldspars

| Material | Initial compounds | Pre-reactions temperature (°C) | Sintering temperature (°C) | Structure (S.G.) |
|---|---|---|---|---|
| $Sr_{0.05}Ba_{0.95}Al_2Si_2O_8$ | $BaCO_3$, $SrCO_3$, $Al_2O_3$, $SiO_2$ | 1000, 1100, 1200, 1300 | 1400–1500 | I2/c |
| $BaAl_2Ge_2O_8$ | $BaCO_3$, $Al_2O_3$, $GeO_2$ | 900, 950, 1000, 1100 | 1300–1450 | I2/c (C2/m) |
| $BaGa_2Si_2O_8$ | $BaCO_3$, $Ga_2O_3$, $SiO_2$ | 1000, 1100, 1200, 1300 | 1300–1420 | I2/c |
| $BaGa_2Ge_2O_8$ | $BaCO_3$, $Ga_2O_3$, $GeO_2$ | 900, 1000, 1100 | 1100–1250 | $P2_1/a$ |

Pre-reaction and sintering time at each temperature was 12 h.

sities were calculated from the formula weight and the unit-cell volume, and the relative densities were obtained by comparing the measured densities with the theoretical ones. For each composition the densities of at least three samples were tested. The average values are reported in Section 3.

The powders obtained by crushing the pellets were examined by infrared spectroscopy using the standard KBr technique. The spectra were recorded at room temperature using a BOMEM MB Series FTIR spectrometer (ABB Bomen, Canada) with a resolution of 2 $cm^{-1}$.

The microstructural studies of the samples were conducted with a scanning electron microscope (SEM) JXA 840A, JEOL, Tokyo, Japan coupled with an energy-dispersive X-ray spectrometer (EDX) and software (Series II X-ray microanalyzer, Tracor Nothern, Middleton, WI).

A transmission electron microscope (TEM) JEOL JEM 2100, equipped with a Gatan ORIUS SC1000 CCD camera, was utilized to compare the tetrahedral ordering of the $Sr_{0.05}Ba_{0.95}Al_2Si_2O_8$ samples. Prior to the TEM investigation the samples were cut into 3-mm-diameter discs, ground to a thickness of approximately 120 μm, dimple ground to 20 μm and ion milled to electron transparency using Ar ions at 3.8 kV.

The radio-frequency (RF) dielectric measurements were performed at 1 MHz on In/Ga-plated disk capacitors using a high-precision LCR meter (Agilent 4284 A). The MW dielectric properties were characterized using the $TE_{01\delta}$ mode dielectric resonator method, described by Krupka et al.[14], and a network analyzer (HP 8719C). The permittivity and dielectric loss tangent (tan $\delta$) values were calculated at the resonant conditions ($TE_{01\delta}$ mode). The $Q$ values were calculated from the tan $\delta$ values in accordance with the equation $Q = 1/\tan\delta$. To determine the temperature coefficient of resonant frequency ($\tau_f$) the test cavities were inserted into a temperature-controlled chamber. The dielectric characteristics of the samples were analyzed in the temperature range from 20 to 60 °C. For the dielectric characterization at least two samples for each set of conditions were tested.

## 3. Results and discussion

### 3.1. Synthesis and structural characterization

#### 3.1.1. $Sr_{0.05}Ba_{0.95}Al_2Si_2O_8$

$Sr_xBa_{1-x}Al_2Si_2O_8$ solid solutions exist in monoclinic (celsian) and hexagonal (hexacelsian) modifications. For many technical applications hexacelsian is regarded as an undesirable phase due to its high thermal expansion coefficient and due to the phase transition at ~300 °C (hexagonal to orthorhombic), which is accompanied by a relatively large volume change (3–4%) that can cause microcracks. Even though hexacelsian is a high-temperature polymorph, stable from 1590–1760 °C, it also forms at lower temperatures and transforms to celsian very sluggishly. The hexacelsian phase, which formed during the synthesis of the $BaAl_2Si_2O_8$, did not transform completely to celsian after annealing at 1500 °C for 12 h. Sr and Ca substitutions for Ba are known to accelerate the hexacelsian-to-celsian transformation. However, it is also known that the substitution with Ca and Sr decreases the Qxf values, especially in the case of Ca substitution. We showed in a previous study that the solid solution $Sr_xBa_{1-x}Al_2Si_2O_8$ with $x = 0.05$ exhibited an only 5% lower Qxf value compared to $BaAl_2Si_2O_8$.[11] With the partial substitution of Ba for Sr in $Sr_{0.05}Ba_{0.95}Al_2Si_2O_8$, hexacelsian completely transformed to celsian and the Qxf values remained high.

The details of the phase formation during the synthesis of $Sr_xBa_{1-x}Al_2Si_2O_8$ solid solutions are described elsewhere.[11] The $Sr_{0.05}Ba_{0.95}Al_2Si_2O_8$ solid solution is already formed at 1200 °C, where according to the XRD pattern both hexagonal (hexacelsian) and monoclinic (celsian) forms are present. At 1300 °C hexacelsian is completely transformed to the monoclinic celsian (S.G. I2/c).

#### 3.1.2. $BaAl_2Ge_2O_8$

The synthesis of $BaAl_2Ge_2O_8$, which was performed by the reaction of the initial compounds $BaCO_3$, $GeO_2$ and $Al_2O_3$ at temperatures below the melting point, differed from the synthesis reported in the literature, where $BaAl_2Ge_2O_8$ crystals were prepared by crystallization from the melt.[9,15] A sub-solidus synthesis route was chosen in order to prevent, as much as possible, the evaporation of $GeO_2$. The XRD measurements revealed that the $BaAl_2Ge_2O_8$ phase had already started to form at 950 °C. However, at this temperature, other phases, like $BaGe_4O_9$, $BaAl_2O_4$ and $Al_2O_3$, prevailed (Fig. 1, curve a). At 1000 °C the formation of $BaAl_2Ge_2O_8$ was already complete (Fig. 1, curve b); however, a dense microstructure could only be obtained by sintering at $T_s \geq 1300$ °C. When the surface of the sintered pellet was examined using XRD, the additional diffraction lines of an unknown phase appeared in the XRD pattern. These diffraction lines were previously noted in an XRD pattern collected from the surface of a pellet sintered at 1300 °C. The intensities of these diffraction lines increased with an increase

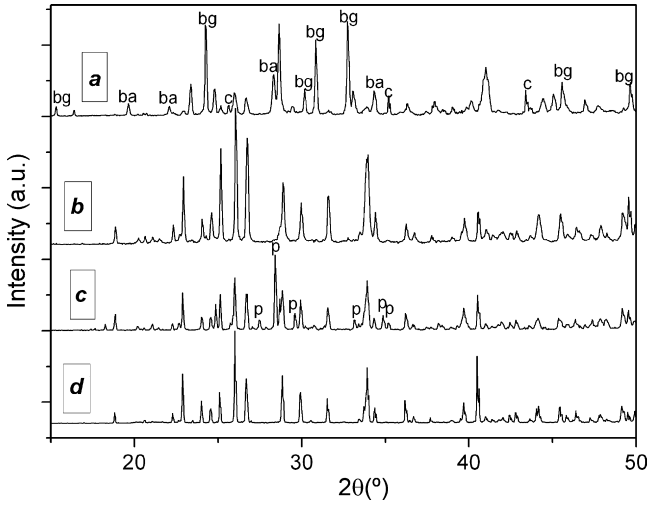


Fig. 1. X-ray diffraction patterns of the samples with a nominal composition of $BaAl_2Ge_2O_8$: (a) powder pre-reacted at 950 °C (bg → $BaGe_4O_9$, ba → $BaAl_2O_4$, c → $Al_2O_3$), (b) powder pre-reacted at 1000 °C, (c) surface of the pellets sintered at 1300 °C (p → unknown phase), (d) surface of the pellet muffled with powder of the composition $BaAl_2Ge_2O_8$ and sintered at 1450 °C (fast cooling).

in the sintering temperature. Within the pellet less or no amount of new phase was observed. On the basis of the mass loss at $T > 1300\,^{\circ}C$, determined with a thermogravimetric analysis, we assumed that this new phase was formed due to the evaporation of $GeO_2$. In order to prevent the $GeO_2$ evaporating the pellets were muffled prior to sintering using powder of the same composition. When using this technique no additional phase was detected on the surface of the pellet sintered at temperatures as high as 1450 °C (Fig. 1, curve d).

The crystal structure of $BaAl_2Ge_2O_8$ fired in the temperature range 1000–1400 °C corresponds to the monoclinic I2/c structure, which was first determined by Calleri and Gazzoni.[15] Later, Malcherek et al. studied in detail the I2/c ↔ C2/m order-disorder phase transition in $BaAl_2Ge_2O_8$.[9,10,16] The ordered distribution of tetrahedral cations leads to the appearance of superstructure b-reflections with $h + k = 2n + 1, l = 2n + 1$ in addition to the basic a-reflections with $h + k = 2n, l = 2n$, which occur in all feldspars.[9] In contrast to the ordering in anorthite and celsian the ordering in $BaAl_2Ge_2O_8$ can also be followed using XRD, due to the different scattering factors of the tetrahedral ions Ge and Al.

### 3.1.3. $BaGa_2Si_2O_8$

The XRD pattern of the sample with the nominal composition of $BaGa_2Si_2O_8$ pre-reacted at 1000 °C consists of several low-intensity diffraction lines that can be attributed to the initial compounds and various barium silicates. However, due to the low intensity and the overlapping of the diffraction lines a complete identification of all of the phases present at this temperature was difficult. Although the XRD pattern of the sample fired at 1100 °C is still complex, the diffraction lines of the monoclinic $BaGa_2Si_2O_8$ (S.G. I2/c) can already be observed, and when the temperature was increased to 1200 °C $BaGa_2Si_2O_8$ became the dominant phase. An unreacted $Ga_2O_3$, which was present in small amounts, was the only secondary phase at this temperature. The diffraction lines that correspond to $Ga_2O_3$ completely disappeared from the XRD pattern of the sample fired at 1300 °C (Fig. 2). Based on this observation we can assume that the $Ga_2O_3$ is similar to $Al_2O_3$, a rather unreactive species. The crystal structure of $BaGa_2Si_2O_8$ synthesized at 1300 °C corresponds to the monoclinic I2/c structure, which was first determined by Calleri and Gazzoni[17] and later by Kroll et al.[18] Their Rietveld structural refinements revealed a mainly ordered distribution of Ga and Si at the tetrahedral sites. In both studies they found some indication of the existence of slight disorder in the tetrahedral sites.[17,18]

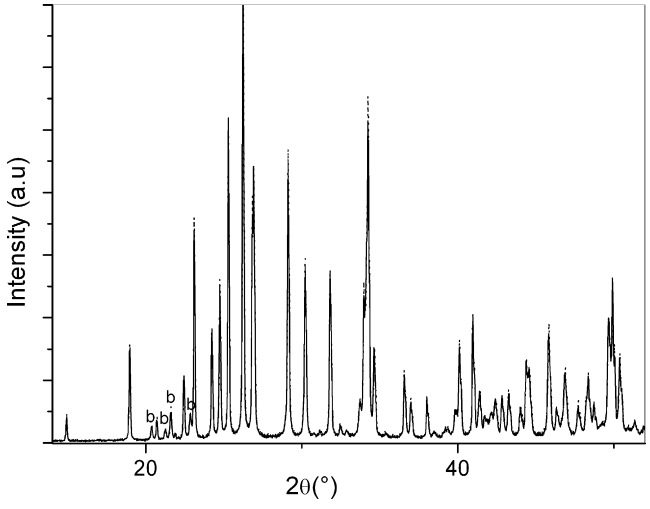


Fig. 2. X-ray powder diffraction patterns of $BaGa_2Si_2O_8$ annealed at 1300 °C (—) and at 1420 °C (⋯⋯). The sample that was annealed at 1420 °C for 50 h was quenched to the room temperature. The b-reflections are denoted with a b.

Table 2
Relative densities of the sintered specimens, determined using Archimedes' method

| Composition | $T_s$ (°C) | Relative density |
|---|---|---|
| $Sr_{0.05}Ba_{0.95}Al_2Si_2O_8$ | 1400 | 98.1 |
| $BaAl_2Ge_2O_8$ | 1300 | 96.4 |
| $BaGa_2Si_2O_8$ | 1300 | 97.5 |
| $BaGa_2Ge_2O_8$ | 1100 | 98.0 |

### 3.1.4. $BaGa_2Ge_2O_8$

Pre-reaction of a mixture with a nominal composition of $BaGa_2Ge_2O_8$ at 900 °C led to the formation of various barium germanium and barium gallium oxides in addition to $BaGa_2Ge_2O_8$. With an increase in temperature to 1000–1100 °C the formation of $BaGa_2Ge_2O_8$ was completed. The structure of $BaGa_2Ge_2O_8$ is monoclinic (S.G. $P2_1/a$), which was reported to be stable over a wide temperature range.[19] From the $BaM_2M'_2O_8$ (M = Al, Ga, M′ = Si, Ge) ceramics $BaGa_2Ge_2O_8$ can be sintered to a good density at the lowest temperature, i.e., at 1100 °C (Table 2).

## 3.2. Structural considerations in correlation with dielectric properties

### 3.2.1. $Sr_{0.05}Ba_{0.95}Al_2Si_2O_8$

A dense ceramic with a relative density higher than 98% (Table 2) was obtained by sintering at 1400–1500 °C. The permittivity showed no significant frequency dispersion from 1 MHz to 10 GHz (Table 3). The sintering temperature and the duration of the heat-treatment were also found to have no significant influence on the permittivity. The measured permittivity of 7.1 was higher than the permittivity ($\varepsilon_s = 5.3$) calculated with the help of the Clausius-Mosotti (C-M) equation and the ion dielectric polarizabilities determined by Shannon.[20] When we made a comparison between the dielectric polarizability determined from the measured permittivity and the dielectric polarizability calculated from the ion dielectric polarizabilities, we observed that this deviation in $Sr_{0.05}Ba_{0.95}Al_2Si_2O_8$ (12%) is similar to that which was already reported for the $CaAl_2Si_2O_8$ ceramic (16.9%).[21]

In contrast to $\varepsilon$ and $\tau_f$, the Qxf values changed with the annealing conditions. The Qxf values increased from 42,500 to 92,600 GHz when the annealing time at 1400 °C increased from 1 to 162 h. The selected-area electron diffraction (SAED) patterns of both samples showed the presence of b-reflections ($h + k = 2n + 1$, $l = 2n + 1$), which confirms their ordered I2/c structure (Fig. 3). Benna et al. in their studies of $SrAl_2Si_2O_8$,

Table 3
The dielectric properties of $Sr_{0.05}Ba_{0.95}Al_2Si_2O_8$, $BaAl_2Ge_2O_8$, $BaGa_2Si_2O_8$, $BaGa_2Ge_2O_8$ feldspars determined at 1 MHz and in the microwave frequency range (at ~12 GHz)

| | Temperature | | | |
|---|---|---|---|---|
| | 1400 °C | | | 1500 °C |
| | 1 h | 12 h | 162 h | 12 h |
| $Sr_{0.05}Ba_{0.95}Al_2Si_2O_8$ | | | | |
| $\varepsilon_{1\,MHz}$ | 7.0 | 7.1 | 7.1 | 7.0 |
| $\varepsilon_{MW}$ | 6.8 | 7.0 (7.0[f]) | 7.0 | 7.2 |
| Qxf (GHz) | 42,500 | 73,500 (64,400[f]) | 92,600 | 83,000 |
| $\tau_f$ (ppm/°C) | −22 | −24 | −22 | −23 |

| | Temperature | |
|---|---|---|
| | 1300 °C 12 h | 1450 °C 12 h |
| $BaAl_2Ge_2O_8$ | | |
| $\varepsilon_{1\,MHz}$ | 7.6 (7.4[f]) | 7.3 (7.2[f]) |
| $\varepsilon_{MW}$ | 7.5 (7.5[f]) | 7.2 (7.0[f]) |
| Qxf (GHz) | 74,100 (50,900[f]) | 50,500 (39,900[f]) |
| $\tau_f$ (ppm/°C) | −32 | −29 |

| | Temperature | | | |
|---|---|---|---|---|
| | 1300 °C 12 h | 1350 °C 12 h | 1400 °C 12 h | 1420 °C 12 h |
| $BaGa_2Si_2O_8$ | | | | |
| $\varepsilon_{1\,MHz}$ | 7.8 | 7.8 (7.7[f]) | 7.7 | 7.6 |
| $\varepsilon_{MW}$ | 7.6 | 7.6 (7.5[f]) | 7.5 | 7.5 |
| Qxf (GHz) | 62,300 | 62,300 (54,700[f]) | 60,400 | 51,700 |
| $\tau_f$ (ppm/°C) | −30 | −32 | | |

| | Temperature | |
|---|---|---|
| | 1100 °C 12 h | 1250 °C 12 h |
| $BaGa_2Ge_2O_8$ | | |
| $\varepsilon_{1MHz}$ | 7.2 (7.1[f]) | 6.8 (6.9[f]) |
| $\varepsilon_{MW}$ | 6.9 (7.0[f]) | 6.8 (6.8[f]) |
| Qxf (GHz) | 106,400 (93,000[f]) | 103,100 (91,900[f]) |
| $\tau_f$ (ppm/°C) | −26 | −26 |

The measurements were performed on the samples that were sintered at the denoted temperature and cooled slowly with a controlled cooling rate of 0.7 °C/min. The values in the brackets represent the results for fast-cooled samples, which is denoted with an f in the superscript.

reported an increase in the size of the ordered domains from an average of 10 nm to approximately 70 nm with an increase in the annealing time from 1.5 to 208 h at 1350 °C.[22] Furthermore, they observed an enlargement of the domains from 200 to 500 nm when the annealing temperature was raised from 1450 to 1640 °C.[23] In our case dark-field images recorded using a 12-1 reflection revealed the presence of antiphase boundaries (APBs), whereas individual, ordered domains could not be clearly distinguished, which implies a high degree of order in both samples (Fig. 4). There is, however, a difference in the concentration of the APBs between the two samples. A comparison of Fig. 4a and b suggests that the area free of APBs is larger in the sample annealed for 162 h than in the one annealed for 1 h. Since antiphase boundaries represent a crystal-structure defect, separating the individual out-of-step ordered domains, this observation implies larger ordered areas in the sample annealed for a longer time. This together with an increase in the tetrahedral order, which according to Benna occurs within individual domains after prolonged annealing, could be the reason for the improvement of the Qxf value.

Benna et al. used infrared spectroscopy (the KBr technique) for the investigations of the local tetrahedral Al, Si ordering in $SrAl_2Si_2O_8$.[22] They noticed a decrease in the linewidth of the vibrational modes at 536 and 623 $cm^{-1}$ with the evolution of the tetrahedral Al, Si order. The linewidth of the corresponding modes decreased on average by ~8 $cm^{-1}$ when the annealing time of the $SrAl_2Si_2O_8$ gels at 1350 °C increased from 0.1 to 452 h. In the $NaAlSi_3O_8$ and $KAlSi_3O_8$ the modes in the spectral range 590–650 $cm^{-1}$ were assigned by Iiishi et al. as O–Si(Al)–O bending modes.[24] In order to detect the difference in the short-range order (SRO) between the samples that differ in terms of Qxf values we used the similar KBr technique.

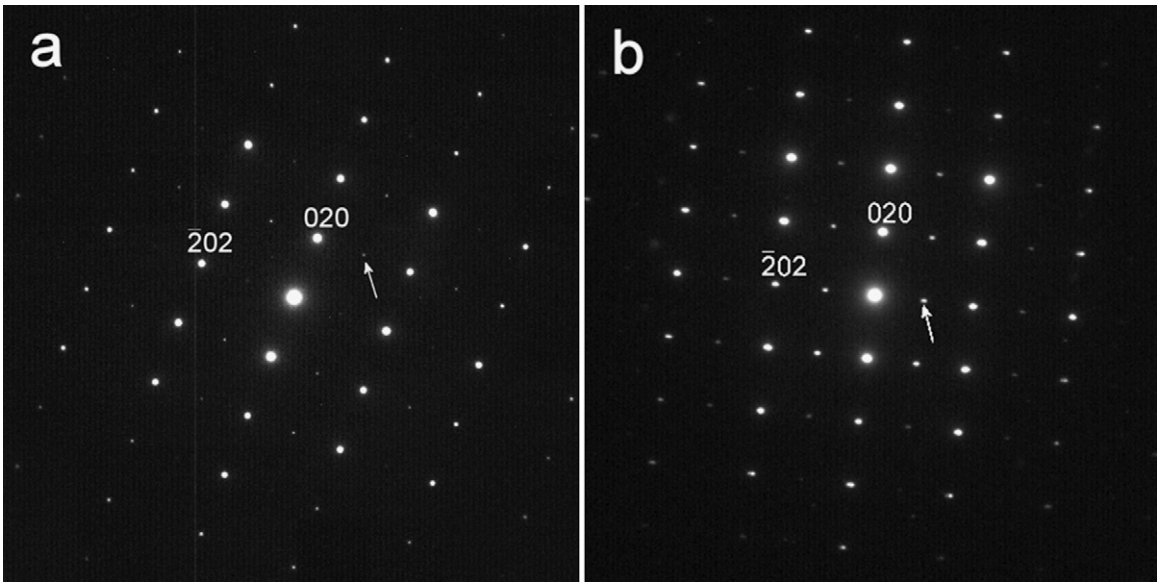


Fig. 3. SAED pattern collected along the [1 0 1] zone axis of $Sr_{0.05}Ba_{0.95}Al_2Si_2O_8$ annealed at 1400 °C for (a) 1 h and (b) 162 h. The arrows indicate the b-reflections.

In spite of the considerable difference in Qxf values there was only a slight difference in the linewidths of the samples. The sample with the higher Qxf value showed a slight but repeatable tendency of a narrower linewidth ($\sim$3 $cm^{-1}$) for the modes in the spectral range 500–750 $cm^{-1}$. Taking into account the decrease in the concentration of the APBs and the decrease in the linewidths of the vibrational modes with annealing, we can assume that the decrease in the concentration of the APBs prevails over the increase in the local tetrahedral order in terms of the Qxf improvement.

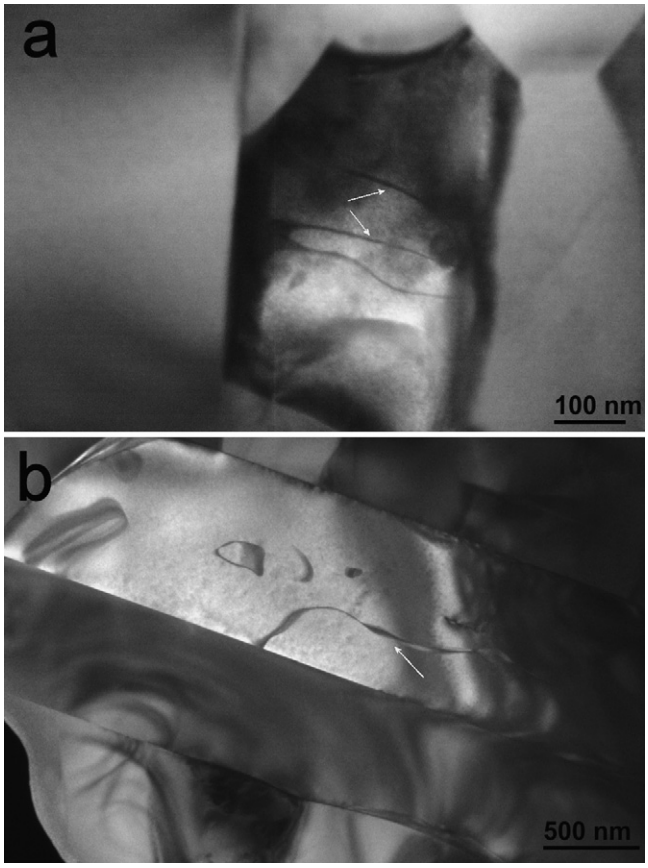


Fig. 4. Dark-field TEM image of $Sr_{0.05}Ba_{0.95}Al_2Si_2O_8$ grains oriented along the [1 0 1] zone axis: (a) 1400 °C/1 h and (b) 1400 °C/162 h, the reflection used is 12-1. The arrows mark the antiphase boundaries.

### 3.2.2. $BaAl_2Ge_2O_8$

For the dielectric characterization the resonators and capacitors were muffled during sintering, i.e., a powder of the same composition covered the pellets in order to suppress the evaporation of $GeO_2$ from the surface. A relative density of the pellets higher than 96% can be obtained by sintering at 1300 °C $\leq T \leq$ 1450 °C (Table 2). Like with $Sr_{0.05}Ba_{0.95}Al_2Si_2O_8$ the measured permittivity of the $BaAl_2Ge_2O_8$ is higher than the predicted permittivity calculated with the C-M equation using the ion dielectric polarizabilities determined by Shannon.[20] The $\tau_f$ of $\sim -30$ ppm/°C, which is slightly more negative than that of $Sr_{0.05}Ba_{0.95}Al_2Si_2O_8$, does not change significantly with temperature (Table 3). In contrast to the permittivity and $\tau_f$, the dielectric losses were expected to be more sensitive to the changes in the structural order caused by the different annealing and cooling conditions. Malcherek et al.[9] showed that the order parameter value of $BaAl_2Ge_2O_8$ decreased with increasing temperature from 0.967 at 900 °C to 0 above the I2/c → C2/m order-disorder phase-transition temperature at 1417 °C. The Qxf values, which decreased with the increase in temperature, showed the similar expected tendency. When the sintering temperature was increased from 1300 to 1450 °C the Qxf values decreased from 74,100 to 50,500 GHz and from 50,900 to 39,900 GHz for the samples cooled slowly and quickly, respectively (Table 3). The higher Qxf values of the slow-cooled samples compared to the fast-cooled ones can be explained by the results of the kinetic study of the C2/m → I2/c phase transition performed by Malcherek et al.[9,10,16] The structure, which became more disordered when the sintering temper-

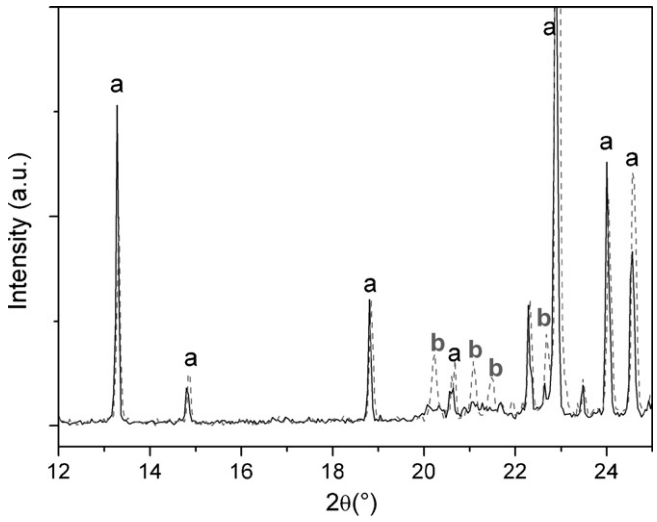


Fig. 5. X-ray diffraction patterns of the pellet surface of $BaAl_2Ge_2O_8$ annealed at 1450 °C for 12 h and then cooled slowly (0.7 °C/min) (– – – –) and quickly (—).

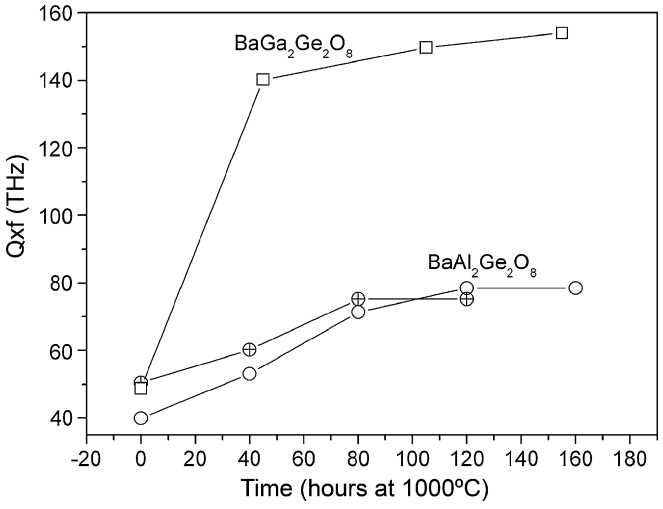


Fig. 6. The increase of Qxf values with annealing at 1000 °C for $BaGa_2Ge_2O_8$ (—□—) (previously annealed at 1250 °C for 60 h) and $BaAl_2Ge_2O_8$ (—⊕—) cooled slowly and $BaAl_2Ge_2O_8$ (—◯—) cooled quickly from the sintering temperature at 1450 °C.

ature exceeded the phase-transition temperature, could order again during slow-cooling. Namely, during cooling with a rate of 0.7 °C/min the ceramics were exposed to temperatures of 900–1300 °C for approximately 10 h. According to the results of Malcherek et al.[9], annealing in this temperature range for such a long time caused a considerable increase in the short- and long-range order parameters. The b-reflections in the XRD pattern of the slow-cooled sample sintered at 1450 °C confirmed the ordering of the structure during cooling. In contrast, fast cooling led to the disappearance of the b-reflections and lower Qxf values (Fig. 5). Taking into account the reported ordering kinetics at 1000 °C it was expected that the Qxf values of the samples sintered above the phase-transition temperature could be improved as a consequence of the increased structural order by annealing at 1000 °C. The Qxf values obtained by prolonged annealing of the disordered samples at 1000 °C were slightly higher than the values obtained for the slow-cooled samples sintered at 1300 °C (Fig. 6, Table 3).

### 3.2.3. $BaGa_2Si_2O_8$

For the measurement of the dielectric properties the ceramics were densely sintered between 1300 and 1420 °C. The relative density was higher than 97% (Table 2). $BaGa_2Si_2O_8$ exhibits a permittivity and $\tau_f$ similar to those values of $BaAl_2Ge_2O_8$. The dielectric measurements revealed a decrease of the Qxf values with an increase in the sintering temperature to 1420 °C (Table 3). Like with the $BaAl_2Ge_2O_8$ the reason for this could be the I2/c → C2/m order-disorder transition. To the best of our knowledge this phase transition in $BaGa_2Si_2O_8$ has not yet been reported. If $BaGa_2Si_2O_8$ undergoes this I2/c → C2/m order-disorder transition it would be reflected in the XRD pattern as a disappearance of the b-reflections. Even when the $BaGa_2Si_2O_8$ samples were annealed at a temperature approximately 10–30 °C below the melting point and quenched no significant difference in the intensity of the b-reflections was observed in the XRD pattern, although a decrease in the Qxf values of more than 50% was noticed (Fig. 2). This proves that the reason for the decrease in the Qxf values with an increase in temperature is not the complete I2/c → C2/m order-disorder phase transition like with $BaAl_2Ge_2O_8$. However, some disordering must have occurred close to the melting point. The formation of a small amount of melt that did not crystallize during the cooling could also cause a decrease in the total $Q$-value. This is due to the relation between the total $Q$ ($Q_t$) and the $Q$ values of the individual components: $Q_t = V_1/Q_1 + V_2/Q_2$. $Q_1$ and $Q_2$ represent the $Q$ values of the components, while $V_1$ and $V_2$ represent the volume fractions of the component.[25]

### 3.2.4. $BaGa_2Ge_2O_8$

Dense, sintered $BaGa_2Ge_2O_8$ ceramics exhibited a permittivity of 7 (Table 3), and like with the I2/c feldspars the measured permittivity was higher than the predicted permittivity calculated with the C-M equation.[20]

The $\tau_f$ of −26 ppm/°C is slightly lower than those of $BaAl_2Ge_2O_8$ and $BaGa_2Si_2O_8$. An ordered distribution of Ga and Ge on the tetrahedral sites is expected in the $P2_1/a$ structure of $BaGa_2Ge_2O_8$. This ordered structure of $BaGa_2Ge_2O_8$ is reflected in high Qxf values over 100,000 GHz. Like with the observations in $BaAl_2Ge_2O_8$ and $BaGa_2Si_2O_8$ the Qxf values showed a tendency to decrease with an increase in the temperature and the cooling rate. The Qxf values decreased considerably after prolonged annealing and fast cooling from temperatures 10–30 °C below the melting point. Like with $BaGa_2Si_2O_8$ this decrease is most probably caused by disordering close to the melting point. When such "disordered" ceramics were annealed for a prolonged time at 1000 °C their Qxf values exceeded the Qxf values of the ceramics sintered at 1100 °C (Table 3, Fig. 6). We should note that we did not observe such an improvement in the Qxf values when the ceramics sintered at 1100 °C were annealed for a prolong time at 1000 °C.

## 4. Conclusions

In this work $Sr_{0.05}Ba_{0.95}Al_2Si_2O_8$, $BaAl_2Ge_2O_8$ and $BaGa_2Si_2O_8$ with the S.G. I2/c, and $BaGa_2Ge_2O_8$ with the S.G. $P2_1/a$, were studied in terms of their dielectric properties and the correlation of these properties with the crystal structure. The permittivities of all the investigated feldspars determined at 1 MHz and in the microwave frequency range were higher ($\varepsilon = 7$–$8$) than the permittivities predicted by the C-M equation ($\varepsilon_s = 5.2$–$5.5$). A similar deviation has already been reported for the $CaAl_2Si_2O_8$ feldspar. Regarding the dependence of the Qxf values on the annealing conditions the aluminosilicate $Sr_{0.05}Ba_{0.95}Al_2Si_2O_8$ feldspars displayed different behaviour to the Ge-containing $BaAl_2Ge_2O_8$ and $BaGa_2Ge_2O_8$ feldspars. The Qxf values of $Sr_{0.05}Ba_{0.95}Al_2Si_2O_8$ increased from 42,500 to 92,600 GHz when the annealing time at 1400 °C increased from 1 to 162 h. The main reason for the improvement of the Qxf value was the decrease in the concentration of APBs with the annealing. From the studied feldspars only $BaAl_2Ge_2O_8$ exhibited a distinct order-disorder I2/c → C2/m phase transition, which resulted in a decrease of Qxf values. Through slow-cooling or additional annealing at 1000 °C the Qxf values could be improved as a consequence of structural ordering. For $P2_1/a$ $BaGa_2Ge_2O_8$ the Qxf values remained in the region of 100,000 GHz for sintering temperatures from 1100 to 1250 °C. By annealing close to the melting point and fast cooling the Qxf value of $BaGa_2Ge_2O_8$ was observed to deteriorate. However, the highest Qxf value of 150,000 GHz was obtained by annealing such Q-deteriorated $BaGa_2Ge_2O_8$ samples at 1000 °C. The $\tau_f$ of all the investigated feldspars was in the range from −20 to −30 ppm/°C.

## Acknowledgement

The authors would like to thank Mr Damjan Vengust for performing the FTIR measurements.

## References

1. Mori, N., Sugimoto, Y., Harada, J. and Higuchi, Y., Dielectric properties of new glass-ceramics for LTCC applied to microwave or milimeter-wave frequencies. *J. Eur. Ceram. Soc.*, 2006, **26**, 1925–1928.
2. Kono, M., Takagi, H., Tatekawa, T. and Tamura, H., High Q dielectric resonator material with low dielectric constant for millimeter-wave applications. *J. Eur. Ceram. Soc.*, 2006, **26**, 1909–1912.
3. Umemura, R., Ogawa, H. and Kan, A., Low temperature sintering and microwave dielectric properties of $(Mg_{3-x}Zn_x)(VO_4)_2$ ceramics. *J. Eur. Ceram. Soc.*, 2006, **26**, 2063–2068.
4. Dai, S. X., Huang, R. F. and Wilcox Sr., D. L., Use of titanates to achieve a temperature-stable low-temperature cofired ceramic dielectric for wireless applications. *J. Am. Ceram. Soc.*, 2002, **85**, 828–832.
5. Koga, E., Yamagishi, Y., Moriwake, H., Kakimoto, K. and Ohsato, H., Large Q factor variation within dense, highly ordered $Ba(Zn_{1/3}Ta_{2/3})O_3$ system. *J. Eur. Ceram. Soc.*, 2006, **26**, 1961–1964.
6. Kolodiazhnyi, T. V., Petric, A., Johari, G. P. and Belous, A. G., Efffect of preparation conditions on cation ordering and dielectric properties of $Ba(Mg_{1/3}Ta_{2/3})O_3$ ceramics. *J. Eur. Ceram. Soc.*, 2002, **22**, 2013–2021.
7. Chai, L. and Davies, P. K., Formation and structural characterization of 1:1 ordered perovskites in the $Ba(Zn_{1/3}Ta_{2/3})O_3$–$BaZrO_3$ system. *J. Am. Ceram. Soc.*, 1997, **80**, 3193–3198.
8. McCauley, R. A., Polymorphism and dielectric electric properties of Ba- and Sr-containing feldspars. *J. Mater. Sci.*, 2000, **35**, 3939–3942.
9. Malcherek, T., Kroll, H., Schleiter, M. and Salje, E. K. H., The kinetics of monoclinic to monoclinic phase transition in $BaAl_2Ge_2O_8$-feldspar. *Phase transitions*, 1995, **55**, 199–215.
10. Malcherek, T., Carpenter, M. A., Kroll, H. and Salje, E. K. H., Cation ordering in $BaAl_2Ge_2O_8$ feldspar: implications for the $I\bar{1} \leftrightarrow C\bar{1}$ phase transition in anorthite. *Phys. Chem. Miner.*, 1999, **26**, 354–366.
11. Krzmanc, M. M., Valant, M. and Suvorov, D., The synthesis and microwave dielectric properties of $Sr_xBa_{1-x}Al_2Si_2O_8$ and $Ca_yBa_{1-y}Al_2Si_2O_8$ ceramics. *J. Eur. Ceram. Soc.*, 2007, **27**, 1181–1185.
12. Krzmanc, M. M., Valant, M., Jancar, B. and Suvorov, D., Sub-solidus synthesis and microwave dielectric characterization of plagioclase feldspars. *J. Am. Ceram. Soc.*, 2005, **88**(9), 2472–2479.
13. Inorganic Crystal Structure Database (ICSD, FindIt, Version 1.4.2.), Faschinformations zentrum (FIZ), Karlsruhe, National Institute of Standards and Technology (NIST), 2007-2.
14. Krupka, J., Derzakowski, K., Riddle, B. and Jarvis, J. B., A dielectric resonator for measurements of complex permittivity of low loss dielectric materials as a function of temperature. *Meas. Sci. Technol.*, 1998, **9**, 1751–1756.
15. Calleri, M. and Gazzoni, G., The structures of (Sr, Ba)[(Al, Ga)$_2$(Si, Ge)$_2$O$_8$]. V. The Crystal structure of the synthetic feldspar $BaAl_2Ge_2O_8$. *Acta Cryst.*, 1977, **B33**, 3275–3282.
16. Malcherek, T., Kroll, H. and Salje, E. K. H., Al Ge cation ordering in $BaAl_2Ge_2O_8$-feldspar: monodomain ordering kinetics. *Phys. Chem. Miner.*, 2000, **27**, 203–212.
17. Calleri, M. and Gazzoni, G., The structures of (Sr, Ba)[(Al, Ga)$_2$(Si, Ge)$_2$O$_8$]. I. The crystal structures of the synthetic feldspars $SrGa_2Si_2O_8$ and $BaGa_2Si_2O_8$. *Acta Cryst.*, 1975, **B31**, 560–568.
18. Kroll, H., Phillips, M. W. and Pentinghaus, H., The structures of the ordered synthetic feldspars $SrGa_2Si_2O_8$, $BaGa_2Si_2O_8$ and $BaGa_2Ge_2O_8$. *Acta Cryst.*, 1978, **B34**, 359–365.
19. Calleri, M. and Gazzoni, G., The structures of (Sr, Ba)[(Al, Ga)$_2$(Si, Ge)$_2$O$_8$]. III. The crystal structures of the Paracelsian-like modifications of synthetic $SrGa_2Ge_2O_8$ and $BaGa_2Ge_2O_8$. *Acta Cryst.*, 1976, **B32**, 1196–1205.
20. Shannon, R. D., Dielectric polarizabilities of ions in oxides and fluorides. *J. Appl. Phys.*, 1993, **73**(1), 348–366.
21. Shannon, R. D., Dickinson, J. E. and Rossman, G. R., Dielectric constants of crystalline and amorphous spodumene, anorthite and diopside and the oxide additivity rule. *Phys. Chem. Miner.*, 1992, **19**, 148–156.
22. Benna, P., Tribaudino, M. and Bruno, E., Al–Si ordering in Sr-feldspar $SrAl_2Si_2O_8$: IR, TEM and single-crystal XRD evidences. *Phys. Chem. Miner.*, 1995, **22**, 343–350.
23. Benna, P. and Bruno, E., Long-range Al, Si equilibrium configuration in Sr-feldspar treated at high temperatures. *Mineralogical Magazine*, 2006, **70**(1), 65–71.
24. Zhang, M., Wruck, B., Barber, A. G., Salje, E. K. H. and Carpenter, M. A., Phonon spectra of alkali feldspars: phase transitions and solid solutions. *Am. Miner.*, 1996, **81**, 92–104.
25. Fukuda, K., Kitoh, R. and Awai, I., Microwave characteristics of $TiO_2$–$Bi_2O_3$ dielectric resonator. *Jpn. J. Appl. Phys.*, 1993, **32**, 4584–4588.